ELSEVIER

Marine and Petroleum Geology 19 (2002) 811–828

Marine and Petroleum Geology

www.elsevier.com/locate/marpetgeo

Depositional environment and source rock potential of Miocene strata from the central Fram Strait: introduction of a new computing tool for simulating organic facies variations

Jochen Knies[a,*], Ute Mann[b]

[a]*Geological Survey of Norway, Leiv Eirikssons vei 39, N-7491 Trondheim, Norway*
[b]*SINTEF Petroleum Research, S.P. Andersen vei 15B, N-7465 Trondheim, Norway*

Received 25 September 2001; received in revised form 12 August 2002; accepted 13 August 2002

Abstract

Organic-rich sediments were recognized in early Miocene strata from the Norwegian-Greenland Sea during ODP Leg 151. Three organic-geochemical subunits were distinguished in Hole 909C using detailed organic-geochemical and microscopic analyses. TOC (up to 3 wt%), HI (up to 200 mg HC/g TOC), and $\delta^{13}C_{org}$ values (~24–26‰) indicate the predominance of terrestrial type III organic matter in Subunit 3 (~18–16.2 Ma). Biomarker and vitrinite reflectance values (R_0 ~ 0.5%) point to rather fresh immature terrestrial organic matter supplied by river discharge from adjacent vegetated coastal areas. Although the sediments of Subunit 3 have a fair (to good) source rock potential they are insufficiently mature to generate significant amounts of oil or gas. To test if the moderate generation potential and source rock quality of Subunit 3 are applicable to the entire area, the computer software OF-Mod was applied. Several modelling runs testing the most probable depositional scenarios result, even under conservative assumptions, in the formation of good to excellent source rocks towards the basin margins.

Keywords: Miocene source rock; Organo facies modelling; Norwegian-Greenland Sea

1. Introduction

In a recent review, Doré, Lundin, Birkeland, Eliassen, and Jensen (1997) stated "there is no firm evidence of a significant contribution from post-Ryazanian source rocks to any petroleum accumulation on the NE Atlantic margin". Nevertheless, the finding of younger source rocks would be of great interest because these rocks could lie at hydrocarbon generation depths today in many basin depocentres in the area (Doré et al.). Indeed, Stein, Brass, Graham, Pimmel, and Shipboard Scientific Party (1995) described a source rock of early to middle Miocene age (later revised to early Miocene; Hull, Osterman, & Thiede, 1996) with a marginal good potential for gas and oil near the bottom of Hole 909C drilled during ODP (Ocean Drilling Program) Leg 151 north of the Hovgård Ridge (78°35.1′N, 03°04.2′E) in the central Fram Strait (Fig. 1) (Myhre, Thiede, & Firth, 1995b). Stein and Stax (1996) proposed a kerogen type II/III for the immature to marginally mature organic matter. In addition, immature, organic-rich layers (TOC: 2–5%) with hydrogen index (HI) values up to 360 mg HC/g TOC accumulated contemporaneously at Site 985 drilled during ODP Leg 162 in the central Norwegian-Greenland Sea (NGS) (Fig. 1; Ikehara, Kawamura, Ohkouchi, & Taira, 1999; Jansen, Raymo, & Blum, 1996) and at Site 645 (ODP Leg 105) in Baffin Bay (Srivastava, Arthur, & Clement, 1987; Stein, 1991a,b; see Fig. 1 for locations). Middle Miocene organic-rich deposits (up to 5.6% TOC) were also detected at Site 642 (ODP Leg 104) on the Vøring Plateau (Fig. 1; Henrich, Wolf, Bohrmann, & Thiede, 1989). Furthermore, Miocene sediments with a strong petroliferous odor were investigated in nearby Site 341 (DSDP Leg 38; Talwani et al., 1975). Although petroleum genesis is indicated to be in an early stage, the overall conclusion was that the sediments do not indicate the presence of anomalously high concentrations of lipids or hydrocarbon substances

* Corresponding author. Tel.: +47-7390-4116.
E-mail address: jochen.knies@ngu.no (J. Knies).

0264-8172/02/$ - see front matter © 2002 Elsevier Science Ltd. All rights reserved.
PII: S0264-8172(02)00090-9

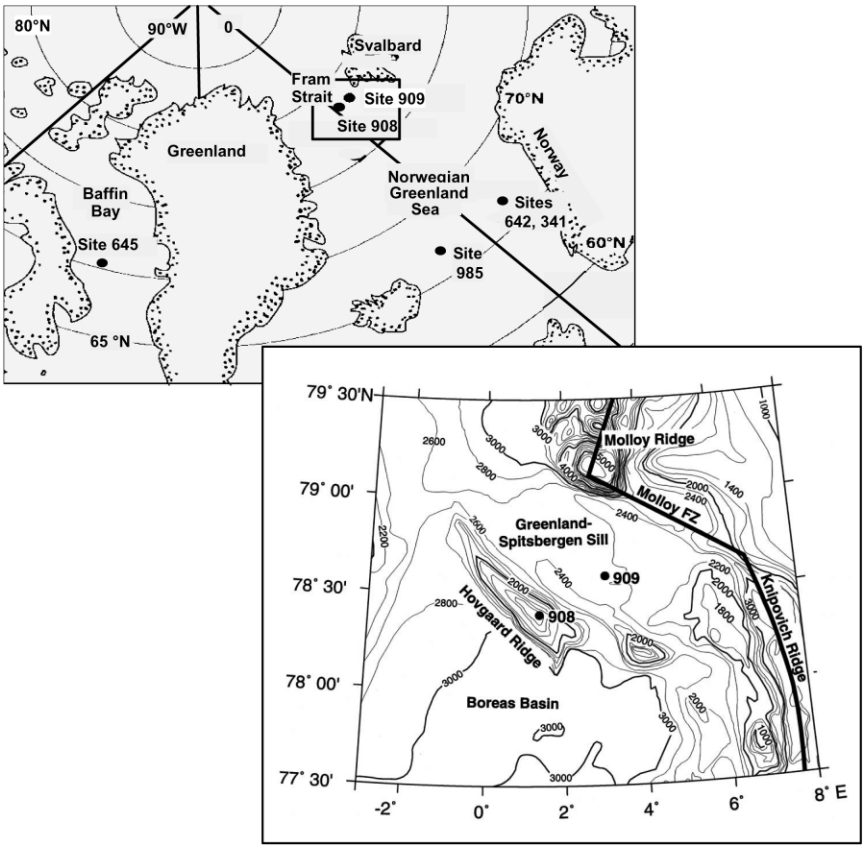

Fig. 1. Keymap showing studied ODP Sites 909 and 908 (central Fram Strait), and discussed Site 645 (Baffin Bay). Detailed map shows the core locations, the bathymetry of the Fram Strait around the Hovgård Ridge, and major plate tectonic structures.

(Kvenvolden, 1976). Nevertheless, the sum of observations in the NGS and the Baffin Bay may suggest a large-scale development of a potential source rock in the area during the early to middle Miocene.

The high concentrations of volatile and liquid hydrocarbons detected in these immature to marginally mature organic-rich sediments near the bottom of Hole 909C are believed to represent mainly migrated material from greater depth (Stein et al., 1995). Their biomarker composition suggested thermal maturity close to the diagenesis/catagenesis boundary, but probably before the onset of thermal hydrocarbon expulsion by cracking of kerogen (Rinna, Rullkötter, & Stein, 1996). However, the possibility that the migrated hydrocarbons were generated from deeper buried, lateral equivalents of these organic-rich Miocene deposits cannot be excluded. The purpose of this paper is therefore to estimate the possible lateral variations in the geochemical indicators regarding the depositional environment and petroleum source rock potential of these early Miocene organic-rich deposits in the central Fram Strait. For this purpose we utilize the OF-Mod (Organic Facies Modelling) software, a computing tool for simulating source rock deposition along 2D basin sections. New detailed organic-geochemical and organic-petrographic studies on lowermost sections of Hole 909C form the framework for the following modeling study.

2. Geologic setting and depositional environment

Recently, Thiede and Myhre (1996) published a detailed summary of the plate tectonic evolution of the NGS. From break-up, Greenland moved in a northwesterly direction with respect to Eurasia, between Anomalies 25 and 24B (~55 Ma) close to the Paleocene/Eocene boundary, and through the Eocene to Anomaly 13 time (~32 Ma) (Fig. 2(a); Talwani & Eldholm, 1977). At the end of the Eocene, a deep basin was created in the southern part of the Greenland Sea, whereas a transpressional regime prevailed along the northern part of the plate boundary between Greenland and Svalbard (Eldholm, Faleide, & Myhre, 1987). Sea-floor spreading stopped in the Labrador Sea and Greenland became part of the American plate at Anomaly 13 time, close to the Eocene–Oligocene transition. Greenland then began to move in a more westerly direction, leading to rifting and finally sea-floor spreading in the northern Greenland Sea (Fig. 2(b)). Myhre and Eldholm (1988) and Myhre, Eldholm, and Sundvor (1982) suggested that the Proto-Hovgård microcontinent was cut off from the Svalbard margin during the opening of the northern Greenland Sea and moved northwestward oblique to the Svalbard margin (Karlberg, 1995; Fig. 2(c)). Based on the extent of the major unconformity at Site 908, between ~25

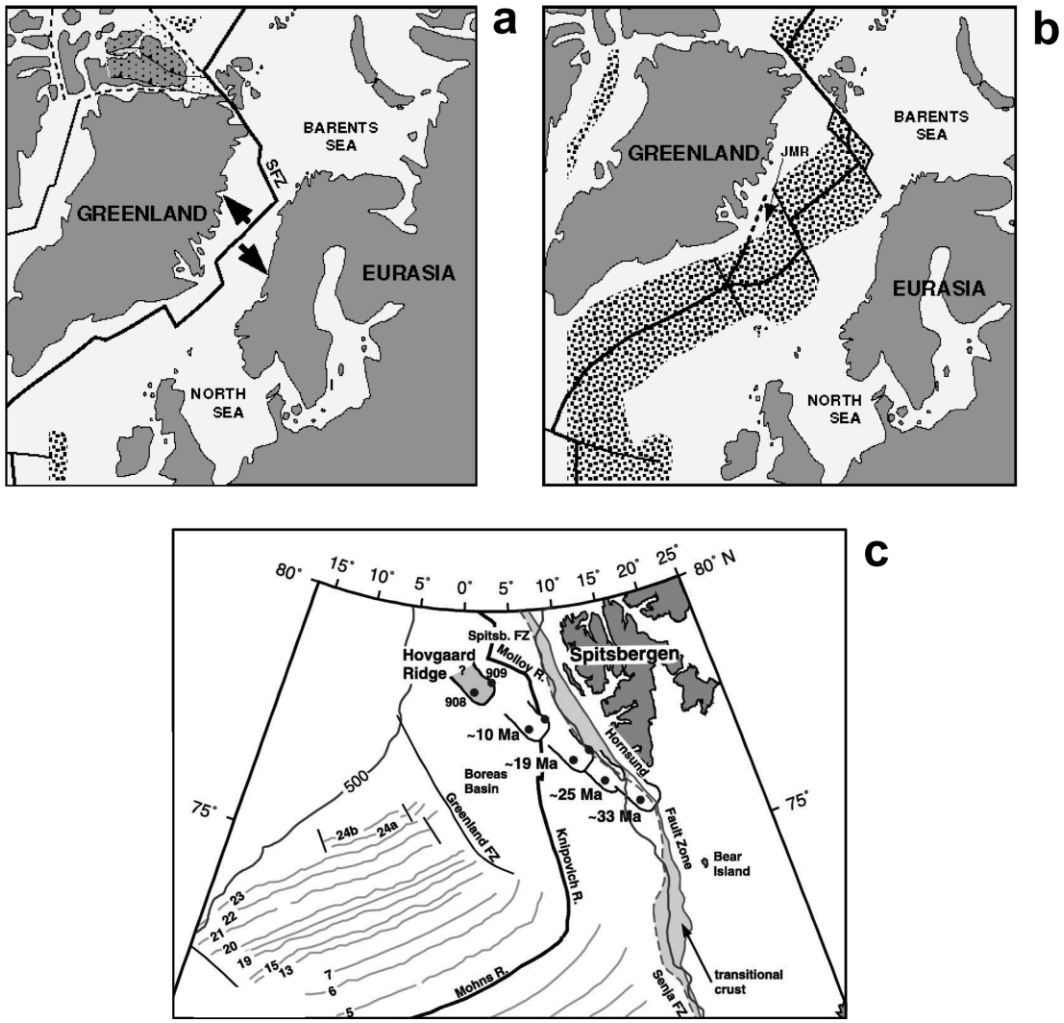

Fig. 2. Schematic plate tectonic reconstructions to the time of break-up, (a) pre-Anomaly 24B time (~55 Ma), (b) Anomaly 13 time (~32 Ma), near the Eocene–Oligocene transition (Myhre et al., 1992). SFZ: Spitsbergen Fracture Zone, JMR: Jan Mayen Ridge. (c) Present-day position of the Hovgård Ridge (with Sites 908 and 909) and its backtracking relative to the Svalbard Platform through time to the Eocene–Oligocene transition. Major plate tectonic structures and paleomagnetic lineations of the Greenland Sea are also shown (adapted from Karlberg (1995)).

and ~10 Ma (Hull et al., 1996), Karlberg in accordance with Myhre, Skogseid, Karlberg, and Eldholm (1995a) suggested an uplift of the ridge above sea level in the last rift phase and subsidence below sea level in late Miocene–early Pliocene times. The deep-water connection to the Arctic Ocean was probably not established before the late Miocene (Kristofferson, 1990; Lawver, Müller, Srivastava, & Roest, 1990) due to the combined effects of continental lithosphere extension prior to sea-floor spreading in the northern Greenland Sea and the influence of transforms within the Spitsbergen Fracture Zone System (Eldholm, Myhre, & Thiede, 1994).

The depositional environment in the central Fram Strait during late Oligocene (25 Ma) and late Miocene (10 Ma) was influenced by riverine input of terrestrially derived, fresh organic matter from the Hovgård Ridge microcontinent (Poulsen, Manum, Williams, & Ellegaard, 1996) and probably from the Svalbard Platform (Hjelstuen, Elverhøi, & Faleide, 1996). The tectonically induced uplift of the Hovgård Ridge above sea-level during this specific time interval (Karlberg (1995) in accordance with Myhre et al., 1982, 1995b) possibly caused non-deposition and erosion of the vegetated coastal areas on the Hovgård Ridge and a huge fluviatile sediment supply in the adjacent basins (Poulsen et al.). Interpretations of cool to temperate climatic conditions and high river discharge are also supported by the high content of smectite (up to 70%) in the clay mineral fraction of the Miocene section of Hole 909C (Winkler, 1999), which is believed to be derived from soil formation on land, e.g. the Svalbard platform and the emerged Barents Sea (Hjelstuen et al., 1996; Winkler, 1999). A similar scenario was proposed for the lower Miocene sediments at Site 645 in the Baffin Bay (Stein, 1991b; for location, see Fig. 1). High accumulation rates of mainly terrestrial organic matter ($0.1\ g\ cm^{-2}\ ka^{-1}$) indicate erosion of dense vegetation cover and fluvial sediment supply from Baffin Island and/or Greenland as a result of a more temperate paleoclimate (Head, Norris, & Mudie, 1989;

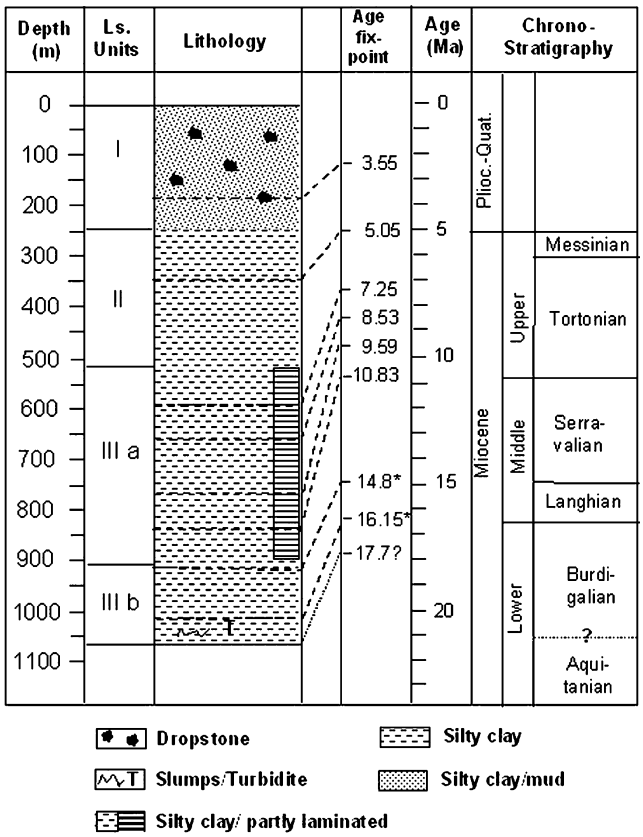

Fig. 3. Lithological units and chronostratigraphy of sediments from Hole 909C (modified after Myhre et al. (1995b)). Age fixpoints are based on paleomagnetic and biostratigraphic data (asteriks) published in Hull et al. (1996), Poulsen et al. (1996) and Wolf-Welling et al. (1996).

Stein, 1991b). The sediments delivered to the western Svalbard margin by fluviatile drainage systems during the Paleocene (~55 Ma) to Pliocene (~2.3 Ma) reach a maximum thickness of 6000 m (Hjelstuen et al., 1996). Sedimentation associated with glacial erosion in the Svalbard/Barents Sea area formed a sedimentary wedge along the western margin, which reaches a maximum thickness of ~4500 m above the Pliocene strata (Faleide, Solheim, Fiedler, Hjelstuen, Andersen, & Vanneste, 1996; Fiedler & Faleide, 1996; Hjelstuen et al., 1996).

3. Regional setting and stratigraphy

The present position of the Hovgård Ridge in the center of the Fram Strait consists of two morphologically different segments offset and separated by a trough (Fig. 1). The northern element (minimum water depth of 1171 m) appears as an elongated, flat-topped, ridge-like feature with a steep southward-facing escarpment. In contrast, the southern segment (1307 m) has a peak-like aspect (Fig. 1). Site 909 is located in the Fram Strait at the Greenland–Spitsbergen Terrace immediate to the northeast of the Hovgård Ridge at a water depth of 2519 m. The Greenland–Spitsbergen Terrace comprises the sill between the Arctic Ocean and the NGS, and is protected against turbidities and slumps originating from the continental margins. Site 909 is located 1246 m below Site 908, which is located on the crest of the Hovgård Ridge at 1273 m water depth (Fig. 1). At Site 909, a 1061 m thick sedimentary section can be subdivided into three major lithologic units (Fig. 3): Unit I (Pliocene to Quaternary) consists of gray to dark gray, silty clays and muds with varying amounts of dropstones; Unit II (late Miocene to Pliocene) contains fewer dropstones and is dominated by very dark gray, silty clay; Unit III (early to late Miocene) was subdivided into Unit IIIa consisting of dark gray, silty clay with meter-scale intervals of bioturbated and laminated layers and Unit IIIb comprised of dark gray, silty clays and containing folded beds and redeposited clasts. Magnetostratigraphy and biostratigraphic zonations were used to date the record (Hull et al., 1996; Myhre et al., 1995b; Poulsen et al., 1996). Unit IIIb, which is the subject of this study, probably comprises a time interval between the ages ~14 and ~18 Ma. However, the exact age of the base is still unknown (earliest Miocene according to Hull

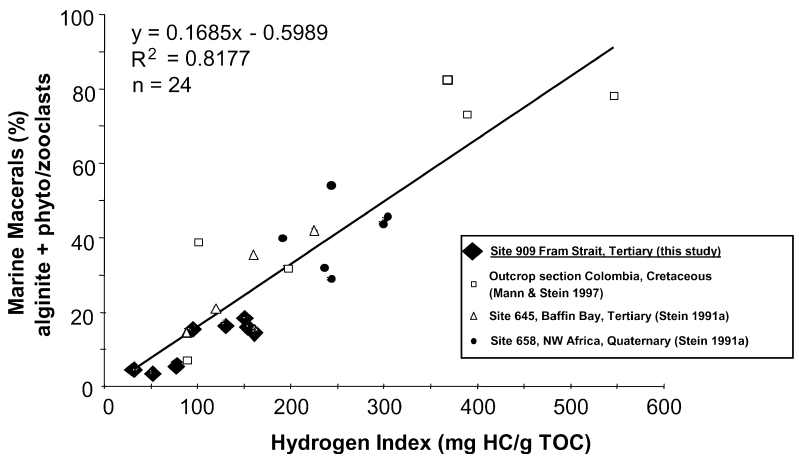

Fig. 4. Correlation between hydrogen index (HI in mg HC/g TOC) and percentages of marine maceral in Hole 909C and selected sites. Tertiary and quaternary ODP Sites 645, Baffin Bay, and 658, NW Africa (Stein, 1991a,b), and Cretaceous black shale section, Colombia (Mann and Stein, 1997). Correlation coefficient ($R^2 = 0.82$) and amount of samples ($n = 24$) used for the correlation are displayed.

Table 1
Results from Rock Eval pyrolysis and kerogen microscopy at Site 909

Core	Sample	Depth (mbsf)	Age (m.y.)	TOC (wt%)	TOM (rel.%)	MOM (rel.%)	LSR (cm/k y)	DBD (g/cm^3)	AR_{TOM} (g/cm^2/k y)	AR_{MOM} (g/cm^2/k yr)	HI (mg HC/g TOC)	PP (gC/m^2 y)	V + H (rel.%)	L (rel.%)	M (rel.%)
909C	083R 3 124-12	879.34	12.05	1.07	1.02	0.05	3.34	1.94	0.07	0.004	33.3	18	90.52	4.49	4.99
909C	086R 1 120-12	905.3	12.82	1.22	1.14	0.08	3.34	1.89	0.08	0.005	39.5	24.7	87.5	6.25	6.25
909C	091R 1 124-12	953.64	14.27	0.79	0.76	0.03	3.34	1.97	0.05	0.002	52.3	12.7	91.27	4.57	4.16
909C	094R 2 124-12	984.04	15.18	1.13	1.06	0.07	3.34	2.05	0.08	0.005	78.4	23.8	86.36	7.07	6.57
909C	099R 1 124-12	1030.44	16.58	1.4	1.34	0.06	3.34	2.18	0.1	0.004	105	22.3	91.38	4.55	4.08
909C	100R 1 31-33	1039.11	16.84	1.44	1.22	0.22	3.34	1.89	0.09	0.014	94.4	50.5	81.78	2.6	15.62
909C	100R 1 140	1040.2	16.87	1.07	0.95	0.12	3.34	1.92	0.07	0.007	117.8	33.2	84.59	4.66	10.75
909C	101R 1 120-12	1049.6	17.15	1.97	1.63	0.34	3.34	2.01	0.13	0.023	130	71.9	79.69	2.9	17.41
909C	102R 2 4-6	1054.24	17.29	1.78	1.44	0.34	3.34	2.21	0.13	0.025	152.3	76.9	78.21	2.79	18.99
909C	102R 2 105-10	1055.24	17.31	2.87	2.43	0.44	3.34	2.21	0.21	0.033	176.7	92.3	81.78	6.13	15.27
909C	102R 3 30-32	1056	17.34	2.7	2.28	0.42	3.34	2.21	0.2	0.031	162.2	89.3	77.85	6.7	15.45
909C	102R 3 121-12	1056.91	17.37	1.51	1.26	0.25	3.34	2.05	0.1	0.017	155.3	58.6	79.64	3.54	16.83

TOC: total organic carbon in wt%, TOM: terrestrial organic matter (rel.%), MOM: marine organic matter (rel.%), LSR: linear sedimentation rate (cm/ka), DBD: dry bulk density (g cm^{-3}), AR_{TOM}: accumulation rate of terrigenous organic matter (g cm^{-2} ka^{-1}), AR_{MOM}: accumulation rate of marine organic matter (in g cm^{-2} ka^{-1}), HI: hydrogen index in mg HC/g TOC, PP: calculated paleoproductivity values (gC m^{-2} a^{-1}), V + H: vitrinite/huminite in %, L: liptodetrinite in %, M: marine alginite including phyto-/zooclasts in %.

et al. (1996)). Some of the age control points are summarized in Fig. 3. Appendix A describes the analytical methods used in this study.

4. Organic matter accumulation rates and paleoproductivity

To avoid misinterpretation of TOC percent values resulting from sediment dilution effects, we calculated linear sedimentation rates and mass accumulation rates of organic carbon (in g cm^{-2} ka^{-1}) using the physical property data and the age control points published by Wolf-Welling, Cremer, O'Connell, Winkler, and Thiede (1996).

By using a combination of HI values and optical maceral composition, we were able to distinguish between marine and terrestrial/reworked organic matter. The correlation of HI values and marine maceral components shown in Fig. 4 is based on a number of different data sets as indicated in the figure captions. Because of the generally good correlation ($R^2 = 0.81$) between these characteristics, we used the amount of marine macerals in Hole 909C sediments to separately estimate the proportions of marine and terrestrial organic matter and to calculate the respective mass accumulation rates (Table 1, Fig. 4).

The next step was to re-estimate, from the marine organic carbon content the surface-water paleoproductivity. Eq. (1) from Mann and Zweigel (2001) was used and is also applied in the modeling program OF-Mod for calculation of marine organic carbon content from productivity data. This equation is based on studies by Betzer, Showers, Laws, Winn, DiTullio, and Kroopnick (1984), Betts and Holland (1991), Johnson-Ibach (1982), Müller and Suess, 1979, and Stein (1991a). The marine organic carbon content in the sediment is controlled by three main processes: (1) the primary productivity of marine organic matter and its flux through the water column; (2) its dilution by inorganic sediment at the sea-bottom; (3) its decomposition/preservation during burial (burial efficiency). These factors are numerically expressed as

$$MOC = \left(\frac{0.409 PP^{1.41} * z^{-0.63}}{10}\right) * \left(\frac{100}{DBD * LSR}\right) * \left(0.54 - 0.54 * \left(\frac{1}{0.037 * LSR^{1.5} + 1}\right)\right) \quad (1)$$

(Organic Carbon Flux; Dilution; Burial Efficiency)

where MOC is marine organic carbon (in %); PP, the primary productivity (in gC m^{-2} a^{-1}); z, the water depth at the time of deposition (in m); DBD, the dry bulk density of sediment (in g cm^{-3}); LSR is the linear sedimentation rate (in cm ka^{-1}).

Solving Eq. (1) for PP allows estimation of the paleoproductivity of the overlying surface water from

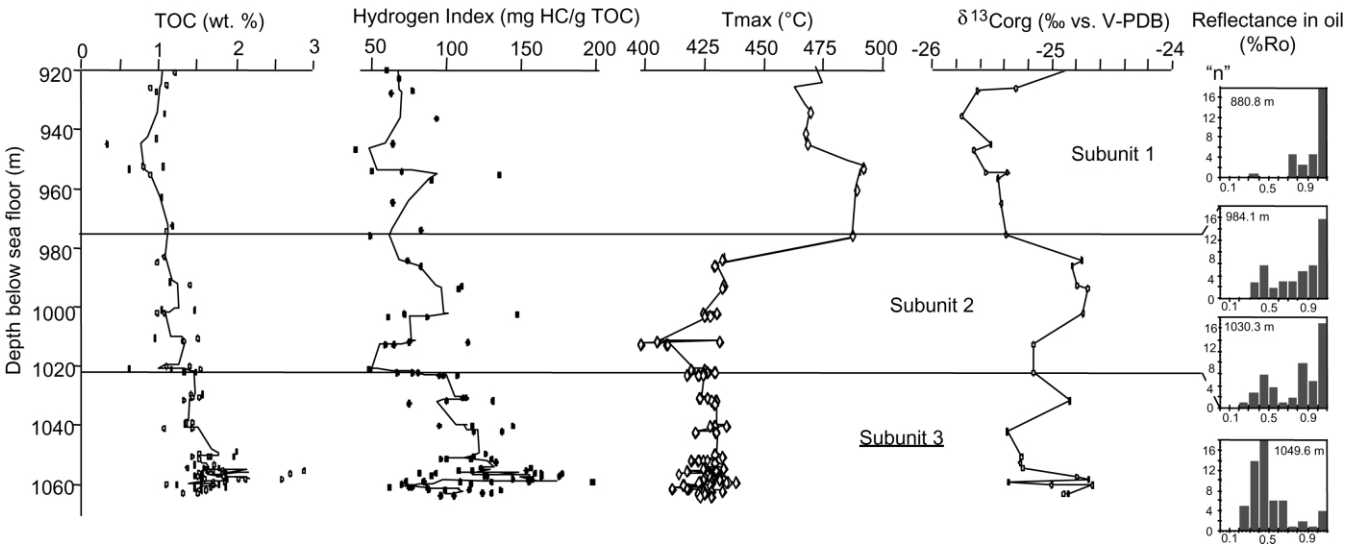

Fig. 5. Results of organic bulk analyses in the three geochemical Subunits of ODP Hole 909C vs. depth (mbsf). TOC: total organic carbon (% of rock weight), hydrogen index (mg HC/g TOC), T_{max}: temperature of maximum pyrolysis yield (in °C), $\delta^{13}C_{org}$: stable carbon isotopes of TOC (in ‰ vs. V-PDB), and vitrinite reflectance histograms of selected samples. Subunit 1 represents the time interval < 14.8 Ma, Subunit 2: 14.8 and ~16.2 Ma, and Subunit 3: ~16.2 and ~17.7 Ma. Trendlines for TOC content and hydrogen index are 3-point moving averages.

sediment data:

$$PP = \left(\frac{MOC \times 0.378 \times DBD \times LSR \times z^{0.63}}{\left(1 - \left(\frac{1}{0.037 LSR^{1.5} + 1}\right)\right)} \right)^{0.71} \quad (2)$$

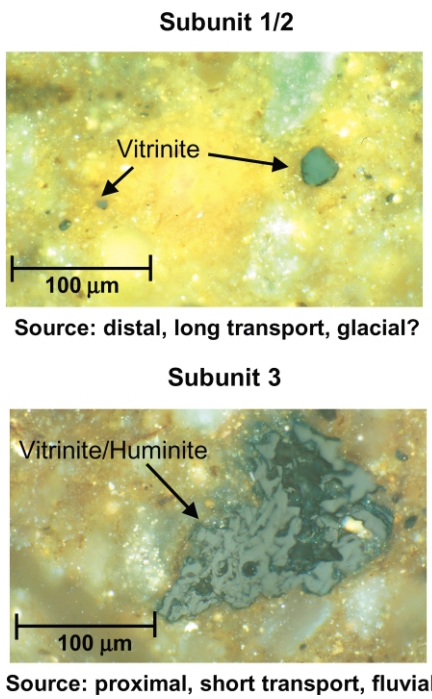

Fig. 6. Photomicrographs showing typical maceral compositions of whole rock samples from Subunits 1/2 and 3. All photos were taken with reflected light under oil immersion. (a) Small and well-rounded vitrinite particles in a light crystalline matrix (Subunit 1/2). (b) Large (>200 µm) dark vitrinite/huminite particle in Subunit 3.

5. Results and discussion

5.1. Sources of organic matter

The lower Miocene strata in Hole 909C (Unit IIIb) can be divided into three geochemical Subunits with respect to the organic matter characteristics (Fig. 5). The average TOC content in Subunits 1 (top of Unit IIIb) and 2 is generally low to moderate (0.5–1.2%). HI values are generally ≤100 mg HC/g TOC. T_{max} values of >460 °C and mean vitrinite reflectance (R_o) of generally >1.0% suggest that the organic matter in Subunit 1 is thermally mature to overmature (Fig. 5). Subunit 2 contains higher percentages of indigenous, immature organic matter as is reflected by lower T_{max} values (<435 °C) and a second smaller maximum at a vitrinite reflectance (R_o) of ~0.5% (Fig. 5). $\delta^{13}C_{org}$ values vary between −25.3 and −25.8‰ in Subunit 1, whereas heavier values (−24.9‰ in average) are recorded in Subunit 2. These data confirm the predominantly terrestrial character of the organic matter in Subunit 2. The microscopic analyses show that the light-colored crystalline matrix in Subunit 1 is dominated by vitrinite, with very low amounts of liptinite and inertinite (Table 1). The vitrinite particles are small, well rounded and gray in color, which may indicate a long transport distance (Fig. 6). Larger particles of well-preserved vitrinites/huminites (>100 µm) are more abundant in Subunit 2 (Fig. 6), reflecting enhanced immature/fresh organic matter input from a probably more proximal source area.

In Subunit 3 (bottom of Unit IIIb), the TOC content reaches a maximum of ~3 wt% (Fig. 5). This increase generally parallels the HI values (up to 200 mg HC/g TOC) suggesting an increased input of better preserved and fresher terrestrial organic matter and/or input of marine organic

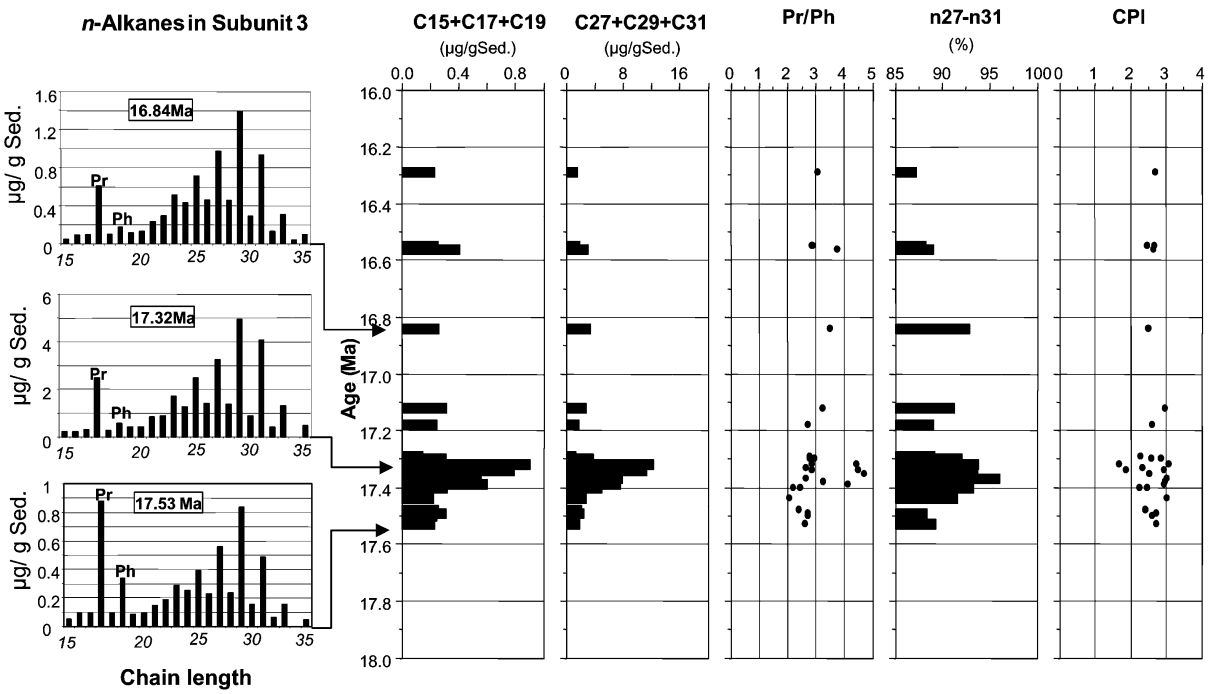

Fig. 7. Left: *n*-alkane distribution (C_{15}–C_{35}) (in µg/g Sed.) of three selected samples in Subunit 3. Pr: pristane, Ph: phytane. Note the dominance of *n*-C_{29} in all samples. Right: hydrocarbon data from Subunit 3 vs. age. $C_{15+17+19}$ = sum of the odd short-chain *n*-alkanes (C_{15}–C_{19}) in µg/g Sed., $C_{27+29+31}$ = sum of the odd long-chain *n*-alkanes (C_{27}–C_{31}) in µg/g Sed., Pr/Ph = pristane/phytane, n_{27}–n_{31} (%) = 100 ($\sum nC_{27}$–nC_{31})/[($\sum nC_{17}$–nC_{19}) + ($\sum nC_{27}$–nC_{29})], CPI: carbon preference index according to Bray and Evans (1961).

matter. T_{max} values of <435 °C and vitrinite reflectance values of R_o 0.4–0.5% indicate thermal immaturity (Fig. 5). Large (>100 µm) particles of vitrinite and huminite dominate the maceral composition in Subunit 3 (Fig. 6), which tends to suggest an even more proximal source for the terrestrial organic matter. Additionally, the proportion of lamalginites (up to 20% of the kerogen) is significantly higher than in Subunits 2 and 1. Terrestrial liptinites and inertinites are negligible in all three Subunits. The overall fresh-looking terrestrial organic matter in Subunit 3 is furthermore geochemically indicated by high pristane/phytane ratios (Pr/Ph = 2–5) and a strong odd-carbon predominance of long-chain *n*-alkanes (C_{27}–C_{31}; Fig. 7) with an average carbon preference index (CPI) value of ~2.7 (Hollerbach, 1985). The total short-chain *n*-alkane (C_{15}, C_{17}, C_{19}) concentrations, representing residues of algae and bacteria (Youngblood & Blumer, 1973), are generally higher in Subunit 3 (0.9 µg/g Sed.) than in Subunit 2 (0.3 µg/g Sed.) (Fig. 7). Furthermore, the dominance of C_{29} steranes (>50%) in the ternary diagram of C_{27}, C_{28}, and C_{29} regular steranes (Fig. 8) is consistent with the microscopically observed high contents of terrestrial organic matter throughout the entire sequence (Huang & Meinschein, 1979), although some ambiguity exists with regard to the application of sterane for interpreting depositional environment (Volkmann, 1986; Volkmann, Barrett, & Blackburn, 1999). High pristane/*n*-C_{17} and phytane/*n*-C_{18} ratios (Pr/*n*-C_{17} > 3; Ph/*n*-C_{18} > 1) confirm the thermal immaturity and also indicate a homogenous source of the terrestrial organic matter and deposition under oxic conditions for Subunit 3 (Fig. 9).

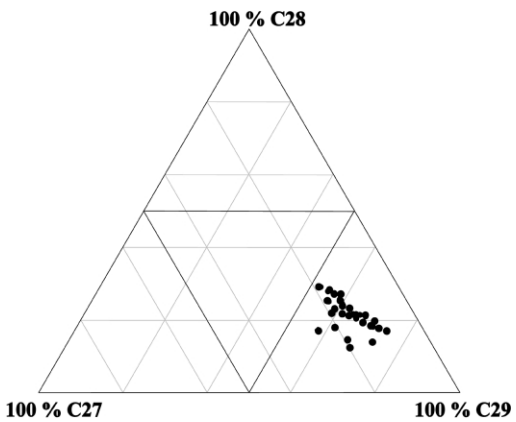

Fig. 8. Carbon number distribution of C_{27}, C_{28}, and C_{29} regular ααα (R + S) + αββ (R + S) steranes from Subunit 3 sediments in Hole 909C [(5α(H), 14α(H), 17α(H) 20S + 20R and 5α(H), 14β(H),17β(H) 20S + 20R)]. The predominance of the C_{29} steranes is consistent with the predominant terrigenous character of the organic matter.

5.2. Quantity of organic carbon and estimated paleoproductivity

Terrestrial and marine organic carbon flux rates and estimated marine paleoproductivity of Miocene strata in the central Fram Strait are shown in Fig. 10. Average accumulation rates of organic carbon are highest in Subunit 3 (up to 0.23 g cm^{-2} ka^{-1}) and decrease to minimum values

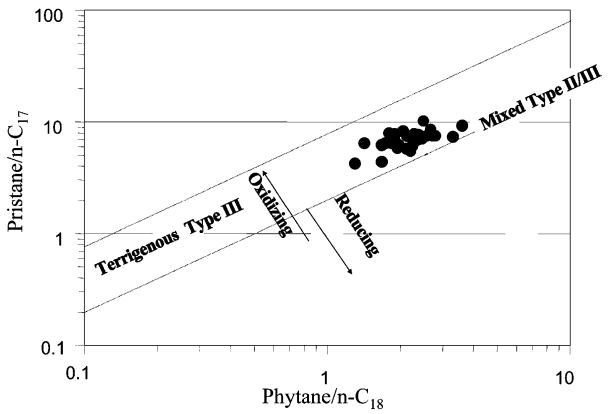

Fig. 9. Pristane/*n*-C_{17} ratio vs. phytane/*n*-C_{18} ratio of rock extracts from Subunit 3 suggesting a homogenous source of the organic matter and deposition under oxic conditions.

in lower part of Subunit 1 (0.03 g cm^{-2} ka^{-1}). A second maximum occurs at the top of Subunit 1 (up to 0.18 g cm^{-2} ka^{-1}). Distinct differences also occur in the type of organic carbon accumulation. The highest accumulation rates of marine organic carbon occur in Subunit 3 (0.03 g cm^{-2} ka^{-1}), together with the highest rates terrestrial organic carbon (up to 0.23 g cm^{-2} ka^{-1}). The lowest marine organic carbon rates were calculated in Subunit 1 (<0.01 g cm^{-2} ka^{-1}). Reworked mature terrestrial organic carbon mainly composes the second maximum of organic carbon accumulation in Subunit 1.

Estimated surface-water paleoproductivity in the central Fram Strait was highest (up to 90 gC m^{-2} a^{-1}) during periods of maximum supply of fresh, immature terrestrial organic matter in Subunit 3 (~17 Ma; Figs. 5, 7, and 10). The high flux rates of fresh terrestrial organic matter suggest dense vegetation and intense fluvial runoff from the Hovgård Ridge and the Svalbard Platform due to humid climatic conditions as already proposed by Boulter and Manum (1996) and Poulsen et al. (1996). Additionally, increased river discharge would imply increased nutrient supply to the ocean, which possibly induced higher surface water productivity and caused higher amounts of marine organic carbon to be deposited under oxic deep-water conditions. The increased fluvial discharge is further supported by high amounts of smectite in the clay fraction of the Miocene section of Hole 909C (up to 70%) indicating erosion and deposition of soil material from the Svalbard Platform and the emerged Barents Sea in the central Fram Strait (Hjelstuen et al., 1996; Winkler, 1999). Moreover, highest productivity values and maximum river discharge in the central Fram Strait during Subunit 3 correlate with the Middle Miocene Climate Optimum (MMCO) at ~17 Ma (Flower & Kennett, 1994), a period of global warming that followed a major glacial episode at the Oligocene/Miocene boundary (Zachos, Flower, & Paul, 1997). According to Shackleton and Kennett (1975), high-latitude surface water temperatures were as much as 6 °C warmer during the MMCO than today. Large polar ice sheets were probably absent (Pagani, Arthur, & Freeman, 1999). The resultant ice-free depositional environment in the central Fram Strait may explain the exclusive sedimentation of fresh terrestrial organic matter from vegetated coastal areas rather than input of reworked and transported organic matter during Subunit 3. Decreasing values in paleoproductivity (down to 20–30 gC m^{-2} a^{-1}) in upper Subunit 3 and input of predominantly reworked and more mature terrestrial organic matter during Subunits 2 and 1 possibly correspond to the termination of the warming period and the initial global cooling between 16 and 12 Ma (Flower & Kennett,

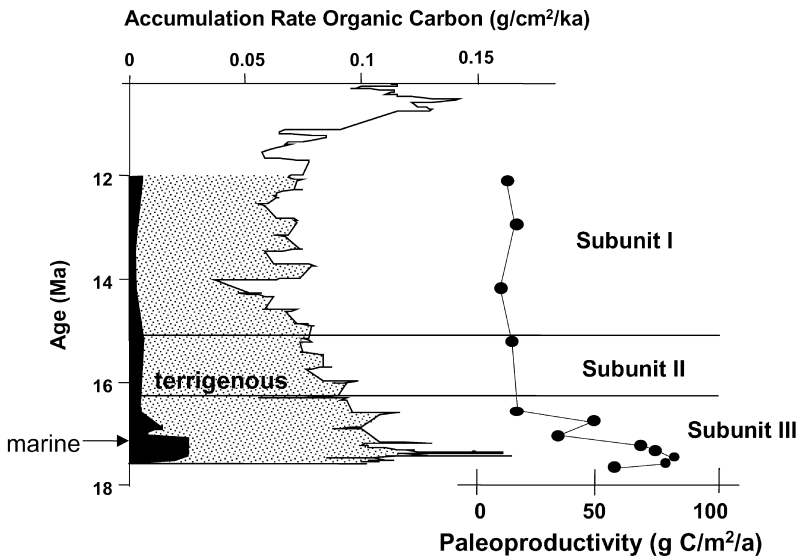

Fig. 10. Left: 3-point moving averages of TOC-accumulation rates of total organic carbon (in g cm^{-2} ka^{-1}) in Hole 909C vs. age. The black filled curve indicates the proportion of marine organic carbon (in g cm^{-2} ka^{-1}) from the total amount. The differences between total and marine organic carbon accumulation rates mark the amount of terrigenous organic proportions. Right: Calculated paleoproductivity shows highest values in Subunit 3 (up to 90 gC m^{-2} a^{-1}) and lowest in Subunits 1 (<30 gC m^{-2} a^{-1}).

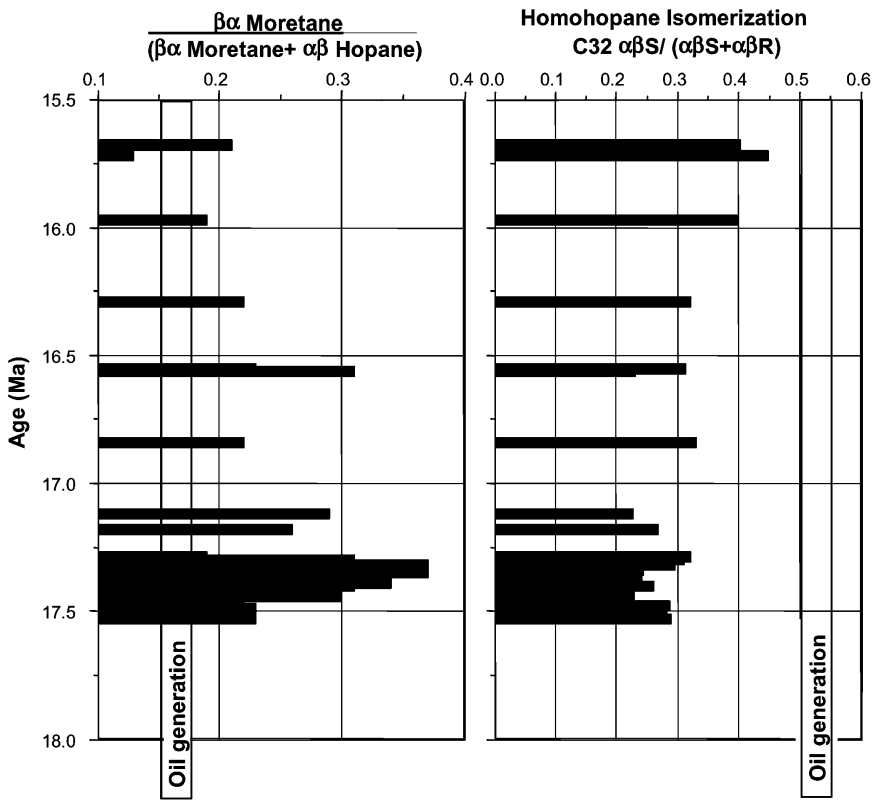

Fig. 11. Moretane/hopane ratio and C_{32} homohopane isomerization (22S/22S + 22R) vs. age of Hole 909C (Subunit 2 and 3). Intervals of initial oil generation are shown (Seifert & Moldowan, 1986). The maturity proxies indicate a rather immature character of the organic matter in sediments of Subunit 3 in the central Fram Strait.

1994). Pulses of ice-rafted debris in the central Fram Strait at ~14 Ma provide evidence of a gradual cooling of the Northern Hemisphere after the MMCO, associated with seasonal and regionally restricted glaciations and sea-ice development (Wolf-Welling et al., 1996). The second maximum in organic carbon flux (up to 0.14 g cm^{-2} ka^{-1}) at ~11 Ma (Fig. 10) in Subunit 1 is mainly represented by reworked terrestrial organic carbon (Stein & Stax, 1996) and coincides with substantial ice-rafting events and intensified ice-build up on the adjacent land masses (Thiede et al., 1998; Wolf-Welling et al., 1996).

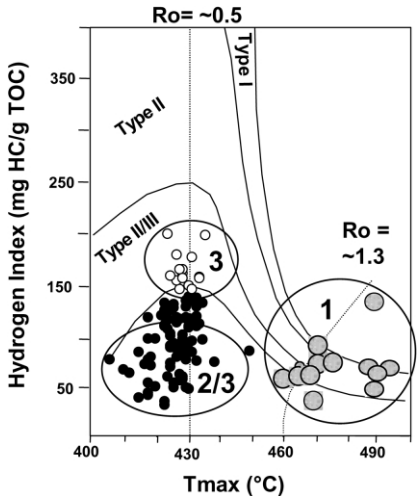

Fig. 12. Rock-Eval hydrogen index vs. T_{max} of early to middle Miocene sediments from Hole 909C. Circles 1–3 mark the corresponding Subunits (1–3) in Hole 909C.

5.3. Petroleum source rock potential

The thermal maturity of Subunit 3 sediments in Hole 909C assessed by vitrinite reflectance (R_0 ~ 0.5%), T_{max} (<435 °C) and production index (PI = S1/(S1 + S2)) values (max 0.18) indicates little in situ petroleum generation (Peters & Moldowan, 1993). Further, the moretane/hopane ratio and C_{32} homohopane isomerization confirm the immature character of the organic material with respect to petroleum generation (Fig. 11). However, according to Peters (1986), the sediments in Subunit 3 of Hole 909C contain enough organic matter (TOC up to 3%, S1 and S2 values of 0.4–0.9, and 2–6 mg HC/g Sed., respectively) to have at least a fair (to good) source rock generative potential. A crossplot of Rock Eval HI and T_{max} values of all Subunits (Fig. 12) point to kerogen type III organic matter (terrestrial) with minor amounts of type II/III (mixed marine/terrestrial) in Subunit 3 suggesting excellent quantities of gas-prone organic matter. Seismic data indicate that more deeply buried Miocene strata from the eastern basin margin are possibly mature with respect to petroleum generation (Hjelstuen et al., 1996). There, a

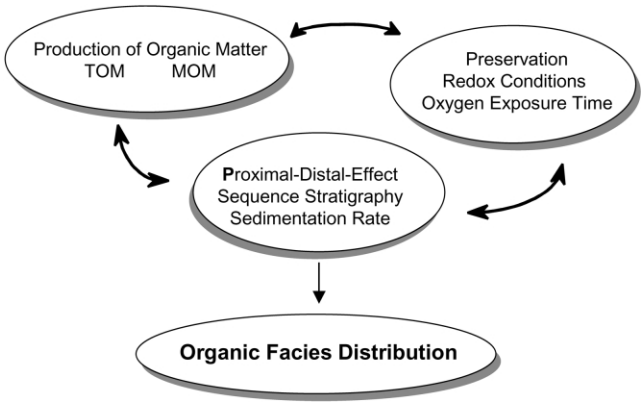

Fig. 13. Main factors influencing organic facies distribution and their interactions. MOM: marine organic matter, TOM: terrigenous organic matter.

sediment wedge three to four times thicker than in the basin center (at Site 909C), was deposited (Hjelstuen et al.). Unfortunately, organic-geochemical studies on Miocene deposits from the basin margins have not been performed so far. Furthermore, there is no control on the thickness of a potential Miocene source rock nor the lateral continuity of Miocene strata with TOC > 2% from the basin center (Site 909) to the margins. However, Bordenave, Espitalié, Leplat, Oudin, and Vandenbroucke (1993) have already argued that deltaic fine-grained sequences with 2–4% TOC and type III kerogen occur regularly and have generated large amounts of gas, condesate, and also oil. Dixon, Dietrich, Snowdon, Morrell, and McNeil (1992) suggested that Tertiary deltaic sediments from the Beaufort-Mackenzie Area with TOC up to 16% and type III kerogen could be the source for oil and gas discovered in Eocene and Oligocene delta-front strata. Very recently, Peters, Snedden, Sulaeman, Sarg, and Enrico (2000) stated, based on a detailed geochemical-sequence stratigraphic study from the Mahakam-Makassar area, Indonesia, that oil-prone source rocks far beyond the coastal plains, i.e. in outer shelf to slope settings, were accumulated due to enhanced erosion of coastal-plain sediments during rapid falls in relative sea level. Indeed, Dunham, Brown, Lin, Redhead, Schwing, and Shirley (2001) found evidence for a terrestrial dominated clastic reworked source rock with up to 15% TOC in the adjacent deepwater Kutai basin, which was originally deposited in deltaic and shallow shelf environments and subsequently transported into deep-water basin by turbidity currents. Although these observations are at odds with conventional source rock models where organic-rich deposits accumulate during periods of low terrestrial-clastic flux or during condensed sequence deposition, there is no doubt that these type III kerogen organic-rich deposits, which originally accumulated in coastal and near-shore environments, are the source for oil and gas accumulations in the Mahakam-Makassar area (Dunham et al., 2001; Peters et al., 2000). In consequence of the fact that the reworked organic matter of type III kerogen is a major contributor to the recent hydrocarbon discoveries on the Makassar slope, Peters et al. proposed that the petroleum potential of deep-water outer shelf and slope areas of kerogen type III petroleum systems worldwide needs to be re-examined.

By comparing the above studies with the present study from the central Fram Strait, we suggest that sediments of Subunit 3—although thermally immature to marginally mature—may contain good quantities of gas and oil-prone organic matter towards the basin margins because of the following arguments: (1) an expected lateral continuity of the Miocene strata with TOC > 2% from the basin center towards the margins, as recent studies from various shelf settings have proven, seems reasonable (Gordon, Goñi, Roberts, Kineke, & Allison, 2001; MacDonald, Solomon, Cranston, Welch, Yunker, & Gobeil, 1998; Stein & Fahl, 2000). (2) A more deeply buried Miocene strata due to a distinctly thicker sedimentary wedge is proven at least for the eastern basin margin (Hjelstuen et al., 1996), and (3) a better quality of the organic matter at the shelf and towards the basin margins seems reasonable because of increasing accumulation of reworked/transported terrestrial organic matter originally supplied by fluviatil drainage systems from the emerged Barents Sea and the Hovgård Ridge (Hjelstuen et al., 1996; Poulsen et al., 1996).

The application of a new computing tool for simulating organic facies variations to the early Miocene strata of the central Fram Strait will further strengthen our arguments for a better Miocene source rock quality towards the basin margins. By using all the available sedimentological, geochemical and tectonic information for reconstructing the depositional environment in the central Fram Strait during early Miocene, we will show that the organo facies model, which was calibrated to the well information from Site 909 located in the central part of the basin, suggests a much better generation potential with respect to petroleum in marginal settings.

6. Basin modeling

To test if the moderate generation potential and source rock quality of Subunit 3 are applicable to the entire basin, the computer software OF-Mod was applied. The program OF-Mod aims to simulate deposition of source rocks and their facies changes along 2D basin sections. Consequently, it allows the quantitative prediction of source rock potential away from well control. The program considers all the principal processes and their interactions controlling the deposition of organic carbon (Fig. 13). OF-Mod has to be linked to a stratigraphic basin-fill program, which provides the model of inorganic deposition needed as input for the organic modelling. For further information on the modelling concept, input and output, and on constraints of the program, we refer to Tømmerås and Mann (1999) and Mann and Zweigel (2001).

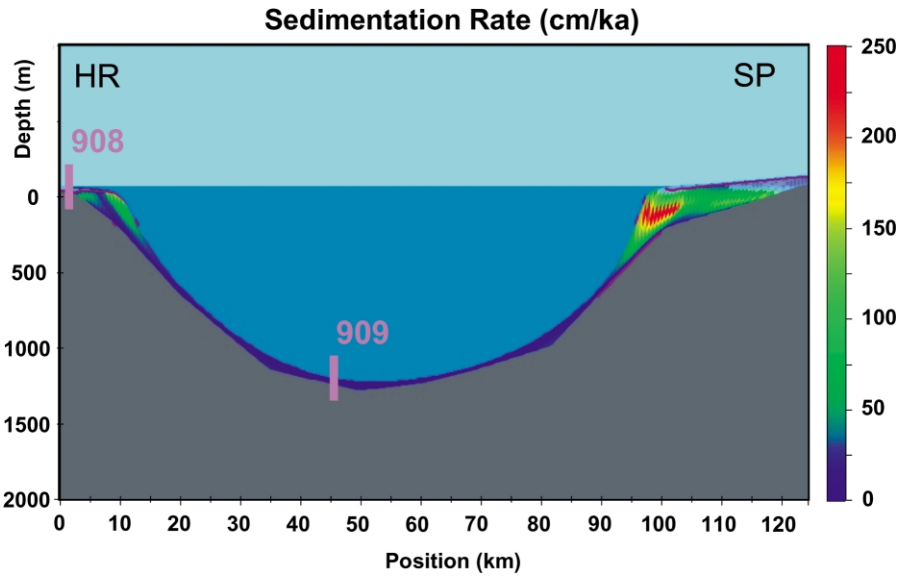

Fig. 14. Reconstructed initial basin geometry between the Hovgård Ridge (HR) and the Svalbard Platform (SP), and modelled sedimentation rate (cm/ka) between ~18 and ~16 Ma (Subunit 3). Locations of Sites 909 and 908 are indicated.

6.1. Background

For the modelling, the reconstruction of the initial basin shape and the depositional history of the organic and inorganic sediment fractions in the central Fram Strait are required. These are based on geological, micropaleontological and geochemical information from ODP Leg 151, Sites 908 and 909. We focused the modeling study on Subunit 3 of Hole 909C (~18–16.2 Ma).

At Site 908, on the crest of the Hovgård Ridge (Site 908), the organic assemblages (pollen, spores, dinoflagellate cysts, plant debris) are dominantly of fresh terrigenous origin (Boulter & Manum, 1996). This indicates a relatively proximal position of Site 908 to forested coastal lowlands probably from the Hovgård Ridge microcontinent itself (Boulter & Manum). The hiatus between ~25 and ~10 Ma in Hole 908A described by Hull et al. (1996) was possibly triggered by tectonically induced vertical movements above sea level (Karlberg, 1995; Myhre et al., 1995a) which caused non-deposition and erosion on the Hovgård Ridge. In Hole 909C the products of these erosion processes, in particular relatively fresh immature terrestrial organic matter (Poulsen et al., 1996), are preserved in Subunit 3. However, according to Poulsen et al. marine basins must have developed east of the Hovgård Ridge because dinocysts from Hole 909C indicate outer neritic conditions during the early Miocene. Hjelstuen et al. (1996) envisaged a system of rivers transporting sediments from the Svalbard Platform and the emerged Barents Sea to the central Fram Strait contributing to the deposition of Subunit 3 in Hole 909C. They suggested an average sedimentation rate of 3.2 cm/ka (max 11.4 cm/ka) along the western Svalbard margin, which is in good agreement with calculated sedimentation rates in Subunit 3 in Hole 909C (~3.4 cm/ka) (Wolf-Welling et al., 1996).

Taking the plate-tectonic reconstruction of the Hovgård Ridge from anomaly 13 (~32 Ma) until today into account (Karlberg, 1995; Fig. 2(c)), we assume the initial basin geometry during deposition of Subunit 3 (~18–16.2 Ma) as outlined in Fig. 14. We suggest, in accordance with Karlberg (1995) and Myhre et al. (1995a) that the Hovgård Ridge crest (Site 908) was emergent above sea level. The water depth at Site 909 was reconstructed by subtracting the present water depths of Sites 908 and 909 from each other assuming constant tectonically induced movement. The distance of the shoreline of the Svalbard Platform to Site 908 (Hovgård Ridge crest) was tentatively estimated from the plate-tectonic reconstruction by Karlberg (Fig. 2(c)). Accordingly, the reconstructed initial basin covers a transect of ~125 km, stretching from the Hovgård Ridge microcontinent in the west into the central part of the basin with a water depth of ~1458 m and up again onto the Svalbard Platform in the east (Fig. 14).

6.2. Software and input data

(1) For the inorganic sedimentation modeling we used DEMOSTRAT (Rivenæs, 1992). This is a 2D, process-based, dynamic-slope type computer program, which employs a dual-lithology, depth-dependent diffusion equation to model deposition and erosion of sand and mud. The program takes initial basin shape, compaction, tectonic and isostatic subsidence as well as eustatic sea-level variations into account. Basement-compaction and -overload can also be considered.

Input data comprised the reconstructed initial basin shape, the eustatic sea-level curve and a sediment compaction curve. These were adopted from Haq, Hardenbol, and Vail (1987) and Baldwin and Butler (1985), respectively. A general assumption was made about the subsidence of the

Table 2
OF-Mod input parameters

		Shore line	
		Left	Right
Marine productivity	PP coastal (gC/m^2/a)	Time varying (200–130)	
	Distance to open ocean (km)	25	40
	PP open ocean (gC/m^2/a)	Time varying (cf. Tab. 1)	
Upwelling induced productivity	δPP (gC/m^2/a)	–	–
	Position (km) from coast	–	–
	Extension of δPP lens (km)	–	–
Terrestrial organic matter	pTOM (%)	Time varying (TOM–SOM)	
	SOM (%) (assumed)	0.2	0.2
Organic matter properties	HI MOM (mg HC/gC)	500	500
	HI pTOM (mgHC/gC)	150	150
	HI SOM (mg HC/gC)	50	50

PP: primary productivity, pTOM: particulate/fresh terrestrial organic matter, SOM: soil organic matter, MOM: marine organic matter, HI: hydrogen index.

basin (20 m/Ma). The isostatic adjustment of the basin within the studied time interval was tentatively estimated. Calculated sedimentation rates in Hole 909C and non-deposition on the Hovgård Ridge crest (Site 908) within the specific time interval (~18–16.2 Ma) were taken as control points for the modeling.

(2) The organic facies simulator OF-Mod models the development and the variations of organic facies along 2D basin transects based on an inorganic sedimentation model, in this case derived from the basin fill program DEMOSTRAT. OF-Mod inversely simulates marine organic carbon deposition: The marine organic accumulation rates

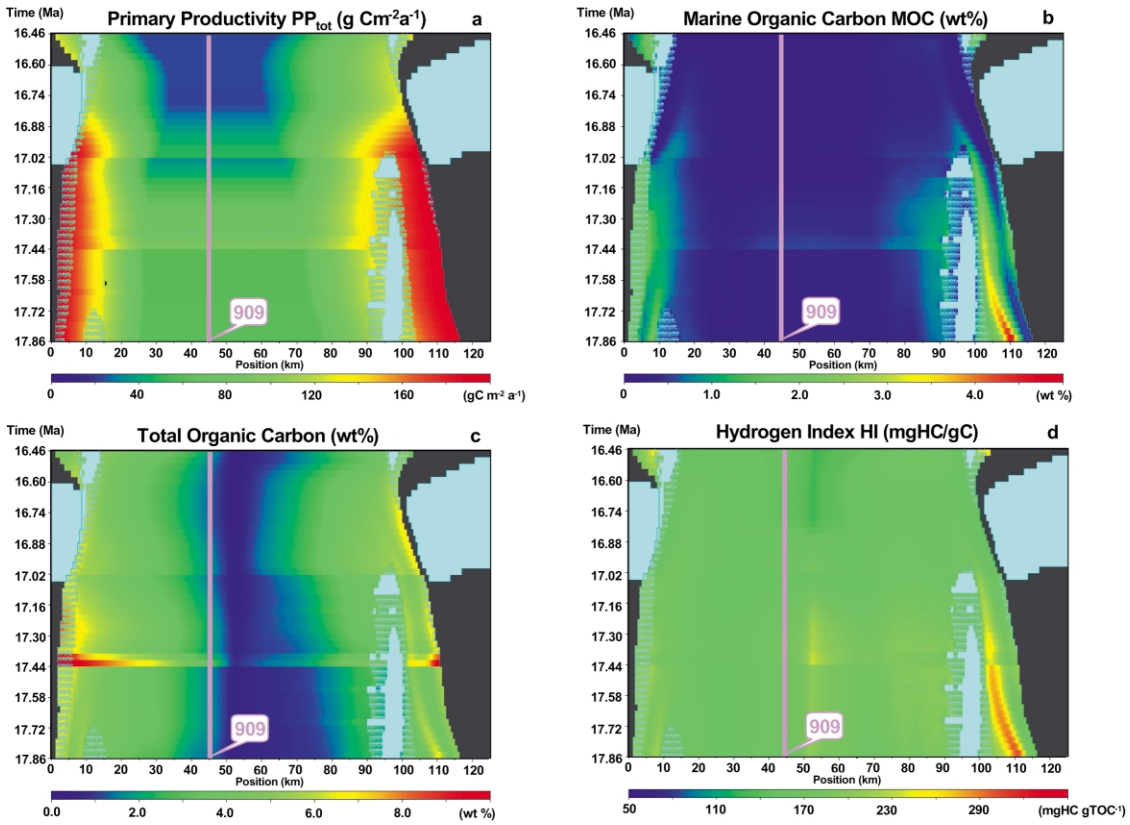

Fig. 15. (a)–(d) Modeling organic facies variations during Subunit 3 (~18–16.2 Ma) in the central Fram Strait between the Hovgård Ridge (HR) and the Svalbard platform (SP) with OF-Mod. Location of Site 909 is displayed. Chronostratigraphic plots of (a) primary productivity (PP$_{tot}$ in gC m^{-2} a^{-1}), (b) marine organic carbon content (MOC in wt%), (c) total organic carbon content (TOC in wt%), and (d) hydrogen index (HI in mg HC/g TOC). For further explanations and discussion see text. Black denotes on shore deposition and is not further differentiated, light blue shows non-deposition, hatched areas indicate later erosion.

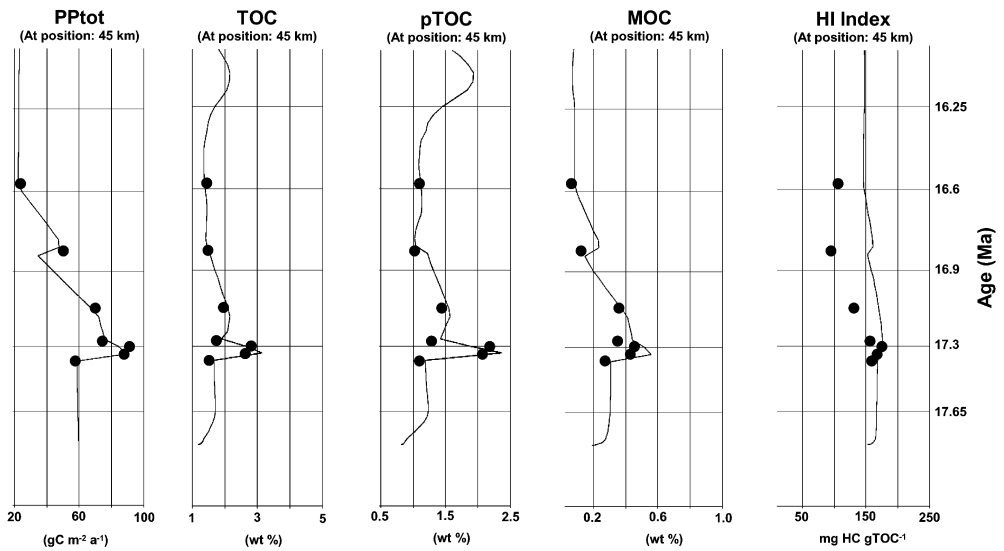

Fig. 16. OF-Mod simulated organic properties (black lines) and measured data points (red dots) in Subunit 3 of Site 909 at position 45 km in the modeled basin. The data are shown in Table 1.

calculated from well data were used to estimate paleo-primary-productivity, which is an input parameter for the modeling. In OF-Mod the distribution of marine primary productivity (PP) is defined as a function of the distance from shore line, e.g. from highly productive coastal waters to low productivity open ocean values. Additionally, an upwelling-induced productivity lens (δPP) can be defined in terms of distance to shore, lateral extent of the lens and intensity of productivity. The normal preservation model considers organic carbon flux in oxic water and bottom conditions. However, two options for enhanced preservation under anoxic conditions can be defined. The development of an oxygen minimum zone as a result of high productivity can be modeled and/or anoxic bottom conditions.

In addition to the marine organic sedimentation, input of terrestrial/allochthonous organic material into the marine system is simulated. Its distribution is coupled to the grain size distribution of the inorganic deposits. Shales are connected with user-defined proportions of reworked/soil organic carbon, and sand is associated with particulate (fresh) terrestrial organic carbon (pTOC). The program further allows modeling of some organic matter properties, such as hydrogen index (HI) and source rock potential.

The input/calibration data for the organic facies modeling were derived from geochemical and micropaleontological studies of Site 909 including calculated amounts of marine and terrestrial organic carbon and estimated paleoproductivity (Table 2) as well as sedimentological properties published by Wolf-Welling et al. (1996).

6.3. Modeling results

Fig. 15(a)–(d) shows the OF-Mod-based chronostratigraphic plots for the modeled paleoproductivity (PP_{tot}), marine and total organic carbon content and hydrogen indices. In Fig. 16 measured data of these parameters from Site 909 are compared to modeled values at the corresponding position (km 45) of the transect. An overall good match between measured data (black dots) and simulated values (black lines) occurs.

Although relatively high PP_{tot} values were modeled in the early phase of deposition of Subunit 3 in the central part of the basin (up to 90 gC m^{-2} a^{-1} at Site 909, corresponding to position 45 km in Figs. 15(a) and 16), only minor amounts of marine organic carbon (up to 0.5%) were modeled to be preserved in the sediments (Figs. 15(b) and 16). During this modeling scenario, an oxic depositional environment was suggested for the entire time interval as this is indicated by biomarker data and Rock-Eval analyses from Site 909 (Fig. 9). Measured marine organic carbon values from Site 909 in the center of the basin confirm the modeled values (Fig. 16) and are in agreement with modern observations where, generally under oxic conditions, the marine organic carbon content is extremely low in deep-sea sediments because of weak resistance to oxic decomposition (Romankevich, 1984).

For the basin margins, however, modeling results could not be validated by well information. As mentioned above, seismic and micropaleontological data were used to reconstruct the depositional environment instead (Hjelstuen et al., 1996; Poulsen et al., 1996). These authors suggested a fluviatile drainage system and coastal erosion from the emerged Barents Sea and the Hovgård Ridge as the main sediment transport mechanisms during deposition of Subunit 3. In such an environment with a high fluvial nutrient supply, surface water productivity in shallow marine areas may reach values up to 10 gC m^{-2} d^{-1} (Lohrenz et al., 1999). Therefore, we used generally accepted modern coastal productivity values (150–250 gC m^{-2} a^{-1}; Romankevich, 1984) as an input value for coastal productivity in OF-Mod. As a consequence, higher marine organic carbon values (1–2% in average)

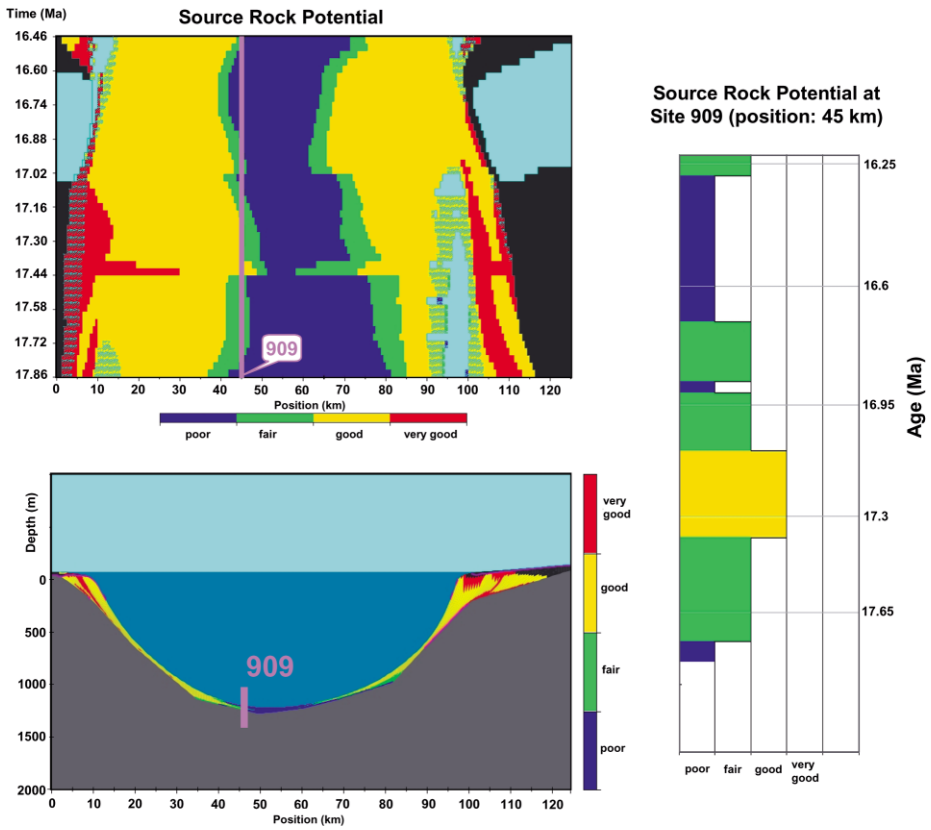

Fig. 17. (a) Chronostratigraphic plot and (b) cross section of simulated variations in source rock potential of the sediments of Subunit 3 between the Hovgård Ridge (HR) and the Svalbard Platform (SP). (c) Log plot of the source rock potential at position 45 km (Site 909) in the modelled basin between ~18 and 16.2 Ma. Note the fair (to good) source rock potential of Subunit 3 as it is indicated by the geochemical data.

were modeled on the shelves rather than in the basin center. Despite possible clastic dilution effects because of the high sediment accumulation along the basin margins, the significantly higher flux of primary produced organic matter in shallow marine areas (<500 mbsf) (Berger, Fischer, Lai, & Wu, 1987; Berger, Smetacek, & Wefer, 1989; Sarnthein, Winn, & Zahn, 1987; Stein, 1991a, after Betzer et al., 1984) and, subsequent rapid burial are potential reasons to explain the higher marine organic carbon values on the shelf and towards the basin margins (Müller & Suess, 1979; Fig. 16(b)).

In parallel, the modeled total organic carbon content (Fig. 15(c)) is also significantly higher on the shelf (4%) and reach values up to 10% towards the coastline. These high coastal values are consistent with observations from the Mahakam Delta, Indonesia, where total organic values (mainly terrestrial derived) of up to 50% in Miocene coastal plain coals and coaly shales occur (Peters et al., 2000).

In our study, the enhanced total organic carbon values of 4–10% mirror mainly the lateral terrestrial organic matter supply from the vegetated coastal areas by river discharge (Boulter & Manum, 1996; Poulsen et al., 1996) rather than higher marine organic carbon flux. Since a terrestrial organic carbon content of up to 2.43% has been calculated previously for the lower part of Subunit 3 in the basin center at Site 909 (Table 1), relatively high amounts of terrestrial organic matter are expected at the basin margins as a consequence of shorter transport distances and proximity to the source area. Relatively constant HI values between 150 and 250 mg HC/g TOC in the basin center (at Site 909) and the margins, respectively, support this suggestion (Fig. 15(d)).

On the other hand, the modeled total organic carbon values of 4–7% in shelf and upper slope deposits diverge somewhat from observations from several modern (Gordon et al., 2001; MacDonald et al., 1998; Stein & Fahl, 2000) and ancient shelf and upper slope settings (Peters et al., 2000) where organic carbon contents are a little lower (1–3%). One reason could be that, despite enhanced terrestrial organic matter supply and increased surface water productivity, high sedimentation rates may result in dilution of the organic material and poorer source rock quality (Johnson-Ibach, 1982; Stein, 1991a). However, Snedden et al. (1996) and Dunham et al. (2001) quite recently found evidence that high amounts of terrestrial organic matter (up to 15%) were also concentrated in outer shelf and slope settings even during periods of high clastic-flux from the shelf. Although no confirmation of 4–8% organic carbon exists along the basin margins, these recent findings from the Mahakam Delta suggest that the modeled organic carbon values of 4–8% in deposits from the shelf and upper slope (Fig. 15(c)) may be reasonable, particularly taking into

account the humid climatic conditions and very proximal position to forested coastal lowlands at the time of deposition (Boulter & Manum, 1996; Poulsen et al., 1996).

To summarize, although the modeled source rock quality of Subunit 3 in the central part of the basin is rather fair (to good) (Fig. 17)—as it is validated by the calibration Site 909—the modeled lateral organic facies variations provide reasonable indications for significant improvement of the source rock quality towards the basin margins during the early to mid-Miocene. This is particularly due to the fact that rapid sedimentation of the organic matter together with high input of terrestrial organic matter by rivers results in organic carbon values that are sufficiently high to indicate good source rock formation along the upper slope and the shelf, as recent observations from the Mahakam Delta have confirmed (Dunham et al., 2001). We believe therefore that the petroleum source rock potential of Subunit 3 along the margins off the Hovgård Ridge and the Svalbard Platform may be good to very good (Fig. 17).

7. Conclusions

Organic-geochemical data from lower to middle Miocene strata in the central Fram Strait reveal substantial stratigraphic variability. The variations mainly reflect changes in the supply of laterally transported terrestrial organic matter and flux of primary produced marine organic matter which were associated with climatic- and tectonic-induced environmental changes. An oxic depositional environment prevailed during deposition of the entire sediment sequence. The lowermost Subunit 3, tentatively dated to ~18–16.2 Ma, contains rather high amounts of fresh, thermally immature, terrestrial organic matter from the adjacent continental margins, the Hovgård Ridge microcontinent and the Svalbard Platform. This high terrestrial input associated with increased nutrient supply via river discharge may have induced enhanced paleoproductivity rates in the entire basin. In the overlying Subunits 2 and 1 (<16.2 Ma), enhanced reworked and thermally mature terrestrial organic matter input possibly transported via sea ice or icebergs. The lowest paleoproductivity rates reflect the initial cooling of the Northern Hemisphere at ~16 Ma.

The potential source rock of fair (to good) quality in Subunit 3 described by Stein et al. (1995) is rather immature and is insufficiently buried to permit significant hydrocarbon generation. However, deeper burial and the occurrence of lateral facies variations in other areas of the basin cannot be excluded. The geological and geochemical data from Site 909 and 908 were used as input/calibration data for the OF-Mod simulator. Several modeling runs applying conservative input parameter estimations and testing the most probable depositional scenarios result in the formation of good to very good source rocks towards the basin margins.

Acknowledgements

We acknowledge the Ocean Drilling Program for providing sample material to perform the study. We are grateful to the staff of the Basin Modelling Department at SINTEF Petroleum Research. In particular, we thank Kristin Lind and Torun Vinge for technical support in the laboratory, Are Tømmerås and Janine Zweigel for discussing the modeling results. Furthermore, we thank Arnim Fluegge, Lutz Schoenicke, and Ulrich Wand for support in the geochemical laboratories of the Alfred Wegener Institute for Polar and Marine Research, Bremerhaven, Germany. Lesley Leith and Hermann Weiss are greatly acknowledged for critical comments to an earlier draft of the manuscript and Olav Eldholm and an anonymous reviewer for formal review. J.K. was financially supported by the German Science Foundation (DFG), grant STE412/11/1.

Appendix A. Methods

A.1. Bulk analysis

Total organic carbon contents of Hole 909C were determined using a Heraeus CHN-analyser (see Stein and Stax (1996) for details). Additional TOC analyses of early Miocene strata were done on powdered whole rocks using a LECO CS 244 analyser. Aliquots (200 mg) of the samples were treated with 10% (vol) hydrochloric acid (HCl) and heated to 60 °C to remove carbonate, and then washed with distilled water to remove all traces of HCl. The samples were dried overnight (50 °C) and then analyzed.

Stable carbon isotopic composition of bulk sediment organic carbon ($\delta^{13}C_{org}$) was determined on carbonate-free (with 10% HCl) samples by high-temperature combustion in a Heraeus Elemental Analyser coupled with a Finnigan MAT Delta S mass spectrometer. The isotopic compositions are reported relative to Vienna-Pee Dee Belemnite (V-PBD). Accuracy was checked by parallel analysis of international standard reference material (IAEA-CH-7). The analytical reproducibility is better than ±0.2‰.

For Rock Eval pyrolysis, aliquots of the crushed samples are weighed into crucibles (~100 mg) and analyzed in a Delsi Rock Eval II instrument under the following conditions (cycle 1): 300 °C isothermally for 3 min, 25 °C/min temperature gradient, 390 °C CO_2 trap shut off, 550 °C isothermally for 1 min (cf. Espitalie et al. (1977) for details). The IFP (Institut Français du Pétrole) Standard 55000 was used to check accuracy of analysis.

Vitrinite reflectance measurements (at least 40 per sample) and macerals analyses were carried out on polished whole rock block sections. The vitrinite reflectance was measured on particles larger than 10 μm under immersion oil at a wavelength of 546 nm. Two standards of known reflectance (0.59 and 0.89%) were used for calibrating the

photometer. The maceral groups vitrinite/huminite, liptinite, and inertinite were classified according to the nomenclature described by Taylor, Teichmüller, Davis, Diessel, Littke, and Robert (1998) (Table 1).

A.2. Biomarker analysis

Aliquots (~3–4 g) of freeze-dried sediment samples were extracted with an acetone/hexane (4:1) mixture by means of high temperature pressurized fluid extraction using an Accelerated Solvent Extractor 200 (Dionex, Salt Lake City). Squalane was added as an internal standard. Saponification was performed using 0.5 M methanolic KOH (95% MeOH + 5% H_2O) at 90 °C for 2 h. Neutral lipids were obtained by extraction with hexane. The separation of saturated hydrocarbons (F1) and nitrogen–sulfur–oxygen organic compounds (NSO) (F2) was employed using a SPE chromatographic column (6 ml, 1 g silica ge/l, Supelco) and sequentially eluting with hexane/dichloromethane (vol, 97:3) (F1), dichloromethane/hexane (vol, 80:20), and methanol (F2).

Gas chromatography of the saturated hydrocarbon fraction was done on a Varian 3400 gas chromatograph (GC-FID) using a fused silica capillary column with dimethyl polysiloxane stationary phase (DB-1, 25 m × 0.32 mm i.d. × 0.2 μm). The temperature program was 80 °C (1 min)—4–6 °C/min—300 °C (20 min). Gas chromatograph–mass spectrometer (GC/MS) analysis were done using a Hewlett-Packard 6890 GC-FID/HP 5973 MSD, and equipped with a Chrompack CP-Sil 5 CB Low bleed, 50 m × 0.25 mm i.d. × 0.25 μm. The GC oven was started at 50 °C (2 min)—35 °C/min—150 °C–2 °C/min—310 °C (12 min). Hydrogen was used as carrier gas. The MS was operated at 70 eV under selected ion mode (*m/z* 99, 177, 183, 191, 205, 217, 218, 231, 232, 253, 259). The sample spectra and mass fragmentograms of triterpanes and steranes were compared with characteristic published spectra and fragmentograms (Peters & Moldowan, 1993).

References

Baldwin, B., & Butler, C. (1985). Compaction curves. *AAPG Bulletin*, *69*, 622–626.

Berger, W. H., Fischer, K., Lai, C., & Wu, G. (1987). Ocean productivity and organic carbon flux. I. Overview and maps of primary production and export production. Technical Report Reference Series 87-30, SIO, Scripps Institution of Oceanography, University of California, USA.

Berger, W. H., Smetacek, V., & Wefer, G. (1989). *Productivity of the ocean: Past and present*. New York: Wiley, 471 p.

Betts, J. N., & Holland, H. D. (1991). The oxygen content of ocean bottom waters, the burial efficiency of organic carbon, and the regulation of atmospheric oxygen. *Palaeogeography, Palaeoclimatology, Palaeoecology*, *97*, 5–18.

Betzer, P. R., Showers, W. J., Laws, E. A., Winn, C. D., DiTullio, G. R., & Kroopnick, P. M. (1984). Primary productivity and particle flux on a transect to the equator at 153°W in the Pacific Ocean. *Deep-Sea Research*, *31*, 1–11.

Bordenave, M. L., Espitalié, J., Leplat, P., Oudin, J. L., & Vandenbroucke, M. (1993). Screening techniques for source rock evaluation. In M. L. Bordenave (Ed.), *Applied petroleum geochemistry, Paris, France* (Technip ed.) (pp. 217–279).

Boulter, M. C., & Manum, S. B. (1996). Oligocene and miocene vegetation in high latitudes of the North Atlantic: Palynological evidence from the Hovgård Ridge in the Greenland Sea (Site 908). In J. Thiede, A. M. Myhre, J. Firth, G. L. Johnson, & W. F. Ruddiman (Eds.), *Proceedings on ODP, Scientific Results* (pp. 289–297). TX, USA: College Station, Ocean Drilling Program.

Bray, E. E., & Evans, E. D. (1961). Distribution of *n*-paraffins as a clue to recognition of source beds. *Geochimica et Cosmochimica Acta*, *22*, 2–15.

Dixon, J., Dietrich, J., Snowdon, L. R., Morrell, G., & McNeil, D. H. (1992). Geology and petroleum potential of upper Cretaceous and Tertiary Strata, Beaufort-Mackenzie Area, Northwest Canada. *AAPG Bulletin*, *76*(6), 927–947.

Doré, A. G., Lundin, E. R., Birkeland, Ø., Eliassen, P. E., & Jensen, L. N. (1997). The NE Atlantic margin: Implications of late Mesozoic and Cenozoic events for hydrocarbon prospectivity. *Petroleum Geoscience*, *3*, 117–131.

Dunham, J. B., Brown, T. J., Lin, R., Readhead, R. B., Schwing, H. F., & Shirley, S. H. (2001). Transport and concentration of gas- and oil-prone kerogens into deep water sediments of the Kutei Basin, East Kalimantan, Indonesia. *AAPG Annual Meeting Program and Abstracts*, Denver Colorado, June 3–6, 2001. p. a54.

Eldholm, O., Faleide, J. I., & Myhre, A. M. (1987). Continent-ocean transition at the western Barents Sea/Svalbard continental margin. *Geology*, *15*, 1118–1122.

Eldholm, O., Myhre, A. M., & Thiede, J. (1994). Cenozoic tectonomagmatic events in the North Atlantic: Potential paleoenvironmental implications. In M. C. Boulter, & H. C. Fischer (Eds.), *Cenozoic plants and climates of the Arctic* (*Vol. 27*) (pp. 35–55). *NATO ASI Series I*, Heidelberg: Springer.

Espitalié, J., Laporte, J. L., Madec, M., Marquis, F., Leplat, P., Paulet, J., & Boutefeu, A. (1977). Méthode rapide de characterisation des roches-mer de leur potential petrolier et de leur degre d'évolution. *Review Inst. Tranc. Petrol.*, *32*, 23–42.

Faleide, J. I., Solheim, A., Fiedler, A., Hjelstuen, B. O., Andersen, E. S., & Vanneste, K. (1996). Late Cenozoic evolution of the western Barents Sea—Svalbard continental margin. *Global Planetary Change*, *12*, 53–74.

Fiedler, A., & Faleide, J. I. (1996). Cenozoic sedimentation along the southwestern Barents Sea margin in relation to uplift and erosion of the shelf. *Global Planetary Change*, *12*, 75–94.

Flower, B. P., & Kennett, J. P. (1994). The middle Miocene climatic transition: East Antarctica ice sheet development, deep ocean circulation and global carbon cycling. *Palaeogeography, Palaeoclimatology, Palaeoecology*, *108*, 537–555.

Gordon, E. S., Goñi, M. A., Roberts, Q. N., Kineke, G. C., & Allison, M. A. (2001). Organic matter distribution and accumulation on the inner Louisiana shelf west of the Atchafalaya River. *Continental Shelf Research*, *21*, 1691–1721.

Haq, B. U., Hardenbol, J., & Vail, P. R. (1987). Chronology of fluctuating sea levels since Triassic (250 Myr ago to present). *Science*, *235*, 1156–1167.

Head, M. J., Norris, G., & Mudie, P. J. (1989). Palynology and dinocyst stratigraphy of the Miocene in ODP Leg 105, Hole 645E, Baffin Bay. In S. P. Srivastava, M. A. Arthur, B. Clement, Shipboard Scientific Party, (Eds.), *Proceedings on ODP, Scientific Results* (pp. 467–514). TX, USA: College Station, Ocean Drilling Program.

Henrich, R., Wolf, T., Bohrmann, G., & Thiede, J. (1989). Cenozoic paleoclimatic and paleoceanographic changes in the Northern Hemisphere revealed by variability of coarse-grained composition in sediments from the Vøring Plateau—ODP Leg 104 Drill Sites. In O. Eldholm, J. Thiede, & E. Taylor (Eds.), *Proceedings on ODP, Scientific Results* (pp. 467–514). TX, USA: College Station, Ocean Drilling Program.

Hjelstuen, B. O., Elverhøi, A., & Faleide, J. I. (1996). Cenozoic erosion and sediment yield in the drainage area of the Storfjorden Fan. *Global Planetary Change*, *12*, 95–118.

Hollerbach, A. (1985). *Grundlagen der Organischen Geochemie*. Berlin: Springer, p. 190.

Huang, W.-Y., & Meinschein, W. G. (1979). Sterols as ecological indicators. *Geochimica et Cosmochimica Acta*, *43*, 739–745.

Hull, D. M., Osterman, L. E., & Thiede, J. (1996). Biostratigraphic synthesis of Leg 151, North Atlantic–Arctic Gateways. In J. Thiede, A. M. Myhre, J. V. Firth, G. L. Johnson, & W. F. Ruddiman (Eds.), *Proceedings on ODP, Scientific Results* (pp. 627–645). TX, USA: College Station, Ocean Drilling Program.

Ikehara, M., Kawamura, K., Ohkouchi, N., & Taira, A. (1999). Organic geochemistry of greenish clay and organic-rich sediments since the early Miocene from Hole 985A, Norway Basin. In M. E. Raymo, E. Jansen, P. Blum, & T. D. Herbert (Eds.), *Proceedings on ODP, Scientific Results* (pp. 209–216). TX, USA: College Station, Ocean Drilling Program.

Jansen, E., Raymo, M. E., Blum, P., Shipboard Scientific Party (1996) (Vol. 162). *Proceedings on ODP, Initial Reports,* TX, USA: College Station, Ocean Drilling Program.

Johnson-Ibach, L. E. (1982). Relationship between sedimentation rate and total organic carbon content in ancient marine sediments. *AAPG Bulletin*, *66*, 170–188.

Karlberg, T. (1995). A geophysical study of the Hovgård Ridge: Cand. cient. Thesis (in Norwegian). University of Oslo, 126 pp.

Kristofferson, Y. (1990). On the tectonic evolution and paleoceanographic significance of the Fram Strait gateway. In U. Bleil, & J. Thide (Eds.), *Geological history of the Polar Ocean: Arctic versus Antarctic* (*Vol. 308*) (pp. 63–76). *NATO ASI Series C*.

Kvenvolden, K. A. (1976). Organic geochemistry, Leg 38: Introduction to studies. In M. Talwani, G. Udintsev, Shipboard Scientific Party, (Eds.), *Initial Reports of the Deep Sea Drilling Project 38, Washington* (pp. 783–784).

Lawver, L. A., Müller, R. D., Srivastava, S. P., & Roest, W. (1990). The opening of the Arctic Ocean. In U. Bleil, & J. Thiede (Eds.), *Geological history of the Polar Ocean: Arctic versus Antarctic* (pp. 29–62). *NATO ASI Series C 308*.

Lohrenz, S. E., Fahnenstiel, G. L., Redalje, D. G., Lang, G. A., Dagg, M. J., Whitledge, T. E., & Dortch, Q. (1999). Nutrients, irradiance, and mixing as factors regulating primary production in coastal waters impacted by the Mississippi River plume. *Continental Shelf Research*, *19*(9), 1113–1141.

MacDonald, R. W., Solomon, S. M., Cranston, R. E., Welch, H. E., Yunker, M. B., & Gobeil, C. (1998). A sediment and organic carbon budget for the Canadian Beaufort Shelf. *Marine Geology*, *144*, 255–273.

Mann, U., & Stein, R. (1997). Organic facies variations, source rock potential, and sea level changes in Cretaceous Black Shales of the Quebrada Ocal, Upper Magdalena Valley, Colombia. *AAPG Bulletin*, *81*, 556–576.

Mann, U., & Zweigel, J. (2001). Modelling organic matter sedimentation. 21st Meeting International Association of Sedimentologists IAS, Davos, Switzerland, 2001, p. 110.

Myhre, A. M., & Eldholm, O. (1988). The western Svalbard margin (74°–80°N). *Marine and Petroleum Geology*, *5*, 134–156.

Myhre, A. M., Eldholm, O., & Sundvor, E. (1982). The margin between Senja and Spitsbergen fracture zones: Implication from plate tectonics. *Tectonophysics*, *89*, 33–50.

Myhre, A. M., Skogseid, J., Karlberg, T., & Eldholm, O. (1995). Tectonic evolution of Fram Strait Gateway in view of ODP Leg 151 results. Fifth International Conference of Paleoceaonography (ICP), Halifax, 1995, Canada (pp. 82–83).

Myhre, A. M., Thiede, J., & Firth, J. V. (1995b) (*Vol. 151*). *Proceedings on ODP, Initial Reports*, TX, USA: College Station, Ocean Drilling Program.

Müller, P. J., & Suess, E. (1979). Productivity, sedimentation rate, and sedimentary organic matter in the oceans. Part I. Organic matter preservation. *Deep-Sea Research*, *26A*, 1347–1362.

Pagani, M., Arthur, M. A., & Freeman, K. H. (1999). Miocene evolution of atmospheric carbon dioxide. *Paleoceanography*, *14*, 273–292.

Peters, K. E. (1986). Guidelines for evaluating petroleum source rock using programmed pyrolysis. *AAPG Bulletin*, *70*, 318–329.

Peters, K. E., & Moldowan, J. M. (1993). *The biomarker guide. Interpreting molecular fossils in petroleum and ancient sediments*. NJ, USA: Prentice Hall, p. 345.

Peters, K. E., Snedden, J. W., Sulaeman, A., Sarg, J. F., & Enrico, R. J. (2000). A new geochemical-sequence stratigraphic model for the Mahakam delta and Makassar slope, Kalimantan, Indonesia. *AAPG Bulletin*, *84*, 12–44.

Poulsen, N. E., Manum, S. B., Williams, G. L., & Ellegaard, M. (1996). Tertiary dinoflagellate biostratigraphy of Sites 907, 908, and 909 in the Norwegian-Greenland Sea. In J. Thiede, A. M. Myhre, J. V. Firth, G. L. Johnson, & W. F. Ruddiman (Eds.), *Proceedings on ODP, Scientific Results* (pp. 255–289). TX, USA: College Station, Ocean Drilling Program.

Rinna, J., Rullkötter, J., & Stein, R. (1996). Hydrocarbons as indicators for provenance and thermal history of organic matter in late Cenozoic sediments from Hole 909C, Fram Strait. In J. Thiede, A. M. Myhre, J. V. Firth, G. L. Johnson, & W. F. Ruddiman (Eds.), *Proceedings on ODP, Scientific Results* (pp. 407–415). TX, USA: College Station, Ocean Drilling Program.

Rivenæs, J. C. (1992). Application of a dual-lithology, depth dependent diffusion equation in stratigraphic simulation. *Basin Research*, *4*, 133–146.

Romankevich, E. (1984). *Geochemistry of organic matter in the ocean*. Berlin: Springer, 334 pp.

Sarnthein, M., Winn, K., & Zahn, R. (1987). Paleoproductivity of oceanic upwelling and the effect on atmospheric CO_2 and climatic change during deglaciation times. In A. L. Berger, & L. Labeyrie (Eds.), *Abrupt Climatic Change* (pp. 311–337). Dordrecht, The Netherlands: Riedel Publications.

Seifert, W. K., & Moldowan, J. M. (1986). Use of biological markers in petroleum exploration. In R. B. Johns (Ed.). *Methods in Geochemistry and Geophysics*, (*Vol. 24*) (pp. 261–290).

Shackleton, N. J., & Kennett, J. P. (1975). Paleotemperature history of the Cenozoic and the initiation of Antarctic glaciation: Oxygen and carbon isotope analyses in DSDP site 277, 279, 281. *Initial Reports Deep Sea Drilling Project* (DSDP) (Vol. 29), pp. 743–755.

Snedden, J. W., Sarg, J. F., Clutson, M. J., Maas, M., Okon, T. E., Carter, M. H., Smith, B. S., Kolich, T. H., & Mansor, M. Y. (1996). Using sequence stratigraphic methods in high-sediment supply deltas: Examples from the ancient Mahakam and Rajang-Lupar deltas: Jakarta. *Proceedings of the Indonesian Petroleum Association*, *25*(1), 281–296.

Srivastava, S. P., Arthur, M., & Clement, B., Shipboard Scientific Party (1987) (*Vol. 105*). *Proceedings on ODP, Initial Reports*, TX, USA: College Station, Ocean Drilling Program.

Stein, R. (1991a). *Accumulation of organic carbon in marine sediments*. Berlin: Springer, 217 p.

Stein, R. (1991b). Organic carbon accumulation in Baffin Bay and paleoenvironment in high northern latitudes during the past 20 m.y. *Geology*, *19*, 356–359.

Stein, R., Brass, G., Graham, D., & Pimmel, A. (1995). Hydrocarbon measurements at Arctic Gateways Sites (ODP Leg 151). In A. M. Myhre, J. Thiede, & J. V. Firth, Shipboard Scientific Party, (Eds.), *Proceedings on ODP, Initial Reports* (pp. 385–395). TX, USA: College Station, Ocean Drilling Program.

Stein, R., & Fahl, K. (2000). Holocene accumulation of organic carbon at the Laptev Sea continental margin (Arctic Ocean): Sources, pathways, and sinks. *Geo-Marine Letters*, *20*, 27–36.

Stein, R., & Stax, R. (1996). Organic carbon and *n*-alkane distribution in late Cenozoic sediments of Arctic Gateways Sites 909 and 911 and their paleoenvironmental implications: Preliminary results. In J. Thiede, A. M. Myhre, J. V. Firth, G. L. Johnson, & W. F. Ruddiman (Eds.),

Proceedings on ODP, Scientific Results (pp. 391–407). TX, USA: College Station, Ocean Drilling Program.

Talwani, M., & Eldholm, O. (1977). Evolution of the Norwegian-Greenland Sea. *Geological Society of America Bulletin*, *83*, 3575–3608.

Talwani, M., Udintsev, G., Bjørklund, K., Caston, V. N. D., Faas, R. W., Kharin, G. N., Morris, D. A., Müller, C., Nilsen, T. H., van Hinte, J. E., Warnke, D. A., & White, S. M. (1975). Leg 38-deep sea drilling Project. *Geotimes*, *20*, 24–26.

Taylor, G. H., Teichmueller, M., Davis, A., Diessel, C. F. K., Littke, R., & Robert, P. (1998). *Organic Petrology*. Berlin: Gebrueder Borntraeger, p. 704.

Thiede, J., & Myhre, A. M. (1996). Introduction to the North Atlantic–Arctic gateways: Plate tectonic—paleoceanographic history and significance. In J. Thiede, A. M. Myhre, J. V. Firth, G. L. Johnson, & W. F. Ruddiman (Eds.), *Proceedings on ODP, Scientific Results* (pp. 3–23). TX, USA: College Station, Ocean Drilling Program.

Thiede, J., Winkler, A., Wolf-Welling, T., Eldholm, O., Myhre, A., Baumann, K.-H., Henrich, R., & Stein, R. (1998). Late Cenozoic history of the Polar North Atlantic: Results from ocean drilling. *Quaternary Science Reviews*, *17*, 185–208.

Tømmerås, A., & Mann, U. (1999). A new approach to simulate the deposition of source rocks at a basin scale. In: S. J. Lippard, A. Naess, & R. Sinding-Larson (Eds.), *Proceedings of IAMG'99, The Fifth Annual Conference of the International Association for Mathematical Geology, (Vol. 2),* ISBN 82-995162-3-4 pp. 569–573.

Volkmann, J. K. (1986). A review of sterol markers for marine and terrigenous organic matter. *Organic Geochemistry*, *9*, 83–100.

Volkmann, J. K., Barrett, S. M., & Blackburn, S. I. (1999). Eustigmatophyte microalgae are potential sources of C29 sterols. C22–C28 *n*-alcohols and C28–C32 *n*-alkyl diols in freshwater environments. *Organic Geochemistry*, *30*, 307–318.

Winkler, A. (1999). The climate history of the high northern latitudes since the Middle Miocene: Indications from sedimentological and clay mineralogical analyses (ODP Leg 151, central Fram Strait). *Reports on Polar Research*, *344*, p. 117.

Wolf-Welling, T. C. W., Cremer, M., O'Connell, S., Winkler, A., & Thiede, J. (1996). Cenozoic Arctic Gateway paleoclimate variability: Indications from changes in coarse-fraction composition. In J. Thiede, A. M. Myhre, J. V. Firth, G. L. Johnson, & W. F. Ruddiman (Eds.), *Proceedings on ODP, Scientific Results* (pp. 515–569). TX, USA: College Station, Ocean Drilling Program.

Youngblood, W. W., & Blumer, M. (1973). Alkanes and alkenes in marine benthic algae. *Marine Biology*, *21*, 163–172.

Zachos, J. C., Flower, B. P., & Paul, H. (1997). Orbitally paced climate oscillations across the oligocene/miocene boundary. *Nature*, *388*, 567–570.